

LMI-based Variable Impedance Controller design from User Demonstrations and Preferences

Alberto San-Miguel, Guillem Alenyà and Vicenç Puig

Abstract—In this paper, we introduce a new off-line method to find suitable parameters of a Variable Impedance Control using the Learning from Demonstrations (LfD) paradigm, fulfilling stability and performance constraints while taking into account user’s intuition over the task. Considering a compliance profile obtained from human demonstrations, a Linear Parameter Varying (LPV) description of the VIC is given, which allows to state the design problem including stability and performance constraints as Linear Matrix Inequalities (LMIs). Therefore, using a solution-search method, we find the optimal solutions in terms of performance according to user preferences on the desired behaviour for the task. The design problem is validated by comparing the execution from the obtained controller against solutions from designs with relaxed conditions for different user preference sets in a 2-D trajectory tracking task. A pulley looping task is presented as a case study to evaluate the performance of the variable impedance controller against a constant one and its agility and leanness on two one-off modifications of the setup using the user preference mechanism. All the experiments have been performed using a 7-DoF KINOVA GEN3 manipulator.

Index Terms—Physical Human-Robot Interaction, Compliance and Impedance Control, Learning from Demonstration, Optimization and Optimal Control

I. INTRODUCTION

GR^{EAT} research efforts are devoted to introduce robots in anthropic domains (both industrial and domestic) for the sake of further enhancing tasks by physically interacting with humans and the environment. This calls for solutions to embed task characteristics for robot execution and to develop means to safely execute the task in an unstructured environment. For the first part, Learning from Demonstrations (LfD) techniques are presented as an intuitive way for non-expert users to teach robots a new task from multiple human-guided demonstrations, from which relevant task information can be extracted [1]. For the second part, Impedance Control (IC) schemes have arose as a trade-off between classical position and force control, such that the relationship between them is tracked instead [2]. This approach is especially relevant in those scenarios where the robot must follow a trajectory but physical interactions (with humans or the environment) might happen or are necessary for task completion. Additionally, many tasks require changing the IC characteristics along time or according to other phenomenon, namely Variable Impedance Control (VIC). Therefore, there has been a recent interest in integral solutions that make use of the LfD paradigm

The authors are with Institut de Robòtica i Informàtica Industrial (IRI), Consejo Superior de Investigaciones Científicas (CSIC) - Universitat Politècnica de Catalunya (UPC), Llorens i Artigas, 4-6, 08028 Barcelona, Spain, (asanmiguel@iri.upc.edu; galenya@iri.upc.edu; vicenc.puig@upc.edu)

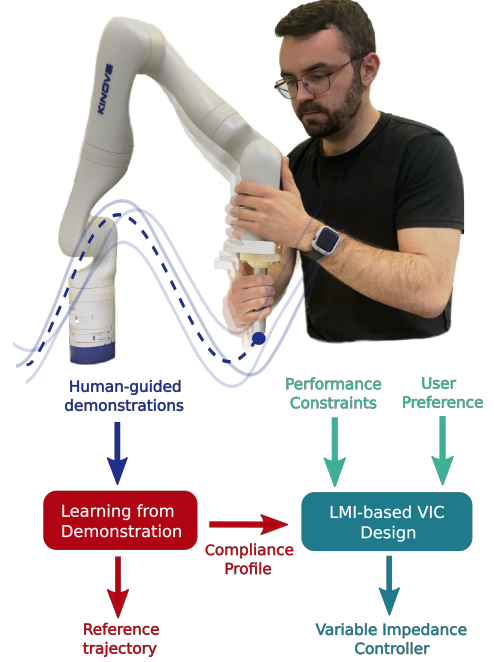


Fig. 1: From human-guided demonstrations, LfD techniques provide the reference trajectory to follow together with the required compliance profile for the task. Our method (LMI-based VIC Design) takes this to derive a set of parameters that define a Variable Impedance Controller (VIC), considering user preference and performance constraints besides stability.

to generate VIC strategies [3]. But, in this intersection of techniques, there is one paramount concern for a safe task execution that is sometimes overlooked: VIC stability and performance, i.e. ensuring that the system will not present improper behaviours while fulfilling some guarantees during the execution of a task.

Therefore, we propose in this paper a novel off-line tuning method to find VIC parameters for modulation profiles generated through LfD techniques, such that a stable closed-loop behaviour is obtained and a set of restrictions on performance are fulfilled, while considering user preference on the compliant behaviour. To do so, VIC is formulated as a polytopic Linear Parameter Varying (LPV) system, which allows to assess both stability and performance constraints using Linear Matrix Inequalities (LMIs). This assessment is performed for all the solutions in the parameter space provided by a solution-search method, considering an optimality score. Additionally, we take into account user preferences (in terms of the desired high and low rigidity to perform the task) to shift the solution-search towards certain regions within the parameter space. This intends to increase the usability of the

method in real tasks by allowing the user to set a desired compliant behaviour. To present this method, we make use of an existing LfD technique proposed by Calinon et. al in [4] to derive task compliance over a time-indexed trajectory as a function of variability between demonstrations. A scheme of the complete method is depicted in Fig. 1.

The paper is organised as follows: Sec. II introduces VIC and the state-of-art on stability assessment together with our previous work and the contributions of this paper. In Sec. III, the VIC structure and the LfD technique are described. The polytopic LPV model formulation for the VIC is outlined in Sec. IV. Sec. V is devoted to the description of the LMI constraints that constitute the design problem. Sec. VI portrays the complete VIC solution generation from LMI problem and User Preference mechanism. Design validation experiments have been included in Sec. VII and Case Study in Sec. VIII.

II. RELATED WORK AND CONTRIBUTIONS

To ensure stability for standard (constant) IC, parameters only have to be positive. For VIC, over the standard IC condition, a much more intricate analysis must be performed to assess this property. Most of the existing literature makes use of methods based on Lyapunov theory, that proves stability through the existence of a suitable candidate function fulfilling a set of conditions [5]. In [6] passivity (which implies stability) conditions are derived from Lyapunov's postulates considering a switching strategy for stiffness modulation of a flexible-joint manipulator. The set of gains used is computed online to fulfil these conditions through a Linear Quadratic Regulator (LQR) problem, which is described by a set of user-defined matrices. Approaches like the one presented in [7] propose state-independent conditions derived from an ad-hoc Lyapunov function to off-line verify the VIC profiles. If we consider assessing also certain performance characteristics of the controller, as e.g. limits on state variables, up to our knowledge, there only exist works on standard IC, as e.g. [8], but not for VIC. Regarding the introduction of stability assessment in controller generation from LfD techniques, we find the i-MOGIC [9] framework for state-varying (function of robot position and velocity) spring-damper controllers (IC without inertia shaping). This is performed at the cost of imposing a modulation strategy based on Gaussian Mixture Regression (GMM) described by user-defined gains.

In our previous work [10], we have already presented the LPV formulation of VIC together with the formalisation of the LMI constraints. Then, w.r.t current state-of-art, our method presents the advantage of being applied online, such that the controller can be designed beforehand and does depend on execution time constraints. Secondly, stability and performance constraints can be applied together such that controller response can fulfil some desired specifications. In this paper, we have broaden this formulation by characterising the VIC according to a LfD technique that provides the level of compliance along a task from a set of user demonstrations. On top of that, a more comprehensive LMI problem has been defined to fine tune the controller response under exogenous forces. Finally, an intuitive mechanism has been introduced

such that users can set their preferences over the compliant behaviour of the VIC.

III. PROBLEM FORMULATION

Impedance Control (IC) aims at imposing a second-order dynamic relationship between (external) forces $\mathbf{F}(\mathbf{t})$ and system position, velocity and acceleration. Considering a 1-DoF trajectory tracking task with references states $\{p^r, \dot{p}^r, \ddot{p}^r\}_{t=0}^T$, system movement is represented by the position error $e := p^r(t) - p(t)$ and its derivatives. Thus, the IC relationship is characterised by a set of parameters, namely inertia H , damping D and stiffness K . Regarding robot compliance, i.e. to which extent the robot movement is affected by interaction forces, stiffness is the most determinant one. Therefore, we are going to put our focus on IC with variant stiffness over time:

$$H \ddot{e} + D \dot{e} + K(t) e = F(t) \quad (1)$$

The approach presented in this paper aims at obtaining the parameters that characterise (1). Regarding the constant ones, we only assume that H is given beforehand, as it is a factor that equally scales D , $K(t)$ and $F(t)$ effects and its value must be determined considering robot hardware [11]. For the variant stiffness, we introduce a description based on a LfD technique. Particularly, we follow the approach presented in [4], where variance in position over different demonstrations for the same trajectory determines the required compliance. Thus, lower variability, i.e. small position differences at the same time, will require a lower compliance, i.e. high movement rigidity. To apply this method, we need to consider a model that embeds all the demonstrations into a single representation. In this paper, we make use of an Heteroscedastic Gaussian Process (H-GP) model adjusted from a standard GP to consider an input-dependant noise [12]. Thus, a set of M position demonstrations p_n^d for times t_n of size T_m conforms the data set $\mathcal{D} = \{\{(t_{m,n}, p_{m,n}^d)\}_{n=1}^{T_m}\}_{m=1}^M$ that is used to train a H-GP defined as $\mathcal{N}(\boldsymbol{\mu}(t), \boldsymbol{\Sigma}(t))$. Then, the eigenvalues $\lambda(t)$ of the inverse covariance matrix $\boldsymbol{\Sigma}^{-1}(t)$ are used to determine the value of K along time:

$$K(t) = K_{min} + (K_{max} - K_{min}) \frac{\log(\lambda(t)) - \log(\lambda_{min})}{\log(\lambda_{max}) - \log(\lambda_{min})} \quad (2)$$

where the values K_{max} and K_{min} are the stiffness parameters to be determined through our tuning method. Also note that reference states are also retrieved from the H-GP model, being $\boldsymbol{\mu}(t) = p^r(t)$ and obtaining \dot{p}^r and \ddot{p}^r through differentiation.

At this point, it is important to note that, although a 1-DoF controller is presented, our method is not limited to a particular number nor a certain combination of DoFs. Also, it should be mentioned that we make use of this particular LfD technique to showcase our approach with a well-understood compliance generation paradigm. But, the proposed approach can be applied to any other technique that generates modulation profiles (function of continuous exogenous signals) and simultaneously modulates any of the parameters.

IV. POLYTOPIC LPV FORMULATION FOR VIC

A. State-space formulation

Considering $\mathbf{x}(t) := [e(t) \ \dot{e}(t)]^T$, we can formulate the impedance relationship from (1) into the state-space form:

$$\dot{\mathbf{x}}(t) = \underbrace{\begin{bmatrix} 0 & 1 \\ 0 & 0 \end{bmatrix}}_{\mathbf{A}_0} \mathbf{x}(t) + \underbrace{\begin{bmatrix} 0 \\ \frac{1}{H} \end{bmatrix}}_{\mathbf{B}_W} \underbrace{\overbrace{[K(t) - D]}^{\mathbf{u}(t)} \mathbf{x}(t)}_{\mathbf{W}(t)} + \underbrace{\begin{bmatrix} 0 \\ \frac{1}{H} \end{bmatrix}}_{\mathbf{B}_F} F(t) \quad (3)$$

being $\mathbf{B}_F(t)$ the force input matrix and $\mathbf{A}(t)$ the (non-linear) state matrix, further divided into a constant value \mathbf{A}_0 and the variant gain $\mathbf{W}(t)$, conforming the controller effort $\mathbf{u}(t)$.

B. LPV Model for VIC

As described in [13], Linear Parameter Varying (LPV) systems are those that can be characterised by a set of varying parameters $\boldsymbol{\theta}(t) = [\theta_1, \dots, \theta_j] \in \mathbb{R}^{n_\theta}$. For system (3):

$$\dot{\mathbf{x}}(t) = \mathbf{A}(\boldsymbol{\theta}(t))\mathbf{x}(t) + \mathbf{B}_F F(t). \quad (4)$$

Each $\theta_j(t)$: (i) needs to be a-priori known, measured or estimated on-line, (ii) must be function of a set of exogenous (i.e. independent of $\mathbf{x}(t)$) signals to the system $\boldsymbol{\zeta}(t) \in \mathbb{R}^\zeta$ and (iii) continuous and defined in the operation range. As shown in (3), $\mathbf{A}(t)$ is defined by one varying parameter:

$$\boldsymbol{\theta}(t) \equiv \theta_1(t) = K(t)/H; \quad (5)$$

In this case, $K(t)$ is: (i) off-line determined from demonstrations given K_{max} and K_{min} , (ii) depends solely on time ($\boldsymbol{\zeta}(t) \equiv \zeta_1 = t$) and (iii) as it is defined from a linear operation over the covariance matrix of a H-GP model, is continuous and defined throughout time (for a non-zero H).

C. Polytopic LPV model from LfD

Properties can be assessed for LPV systems, but dealing with all their (infinite) reachable operating points defined by $\boldsymbol{\theta}(t)$. To make this problem computationally tractable, a polytopic description of the LPV model such that only a set of vertex systems at the operating limits is considered. Formally, all the trajectories of $\boldsymbol{\theta}(t)$ have to be enclosed within the polytope defined by a convex hull $\Theta = \text{Co}\{\theta_{v_1}, \theta_{v_2}, \dots, \theta_{v_N}\}$ with N vertices θ_{v_i} . Each vertex θ_{v_i} one is the combination of the lower and upper bounds of each varying parameter θ_j and $\bar{\theta}_j$, which leads to $N = 2^{n_\theta}$ vertices. To obtain all possible θ_{v_i} , the so-called *bounding box* method [14] can be applied, where maximum and minimum values of each θ_j can be obtained by evaluating them for all the range of ζ_q . The polytopic model of the LPV system can be obtained by evaluating the varying state-space matrices at the convex hull vertices, which leads to the so-called vertex systems. Thus, the polytopic definition of (4) can be obtained by considering the non-negative coefficients $\pi_i(\boldsymbol{\theta}(t))$:

$$\dot{\mathbf{x}}(t) = \sum_{i=1}^N [\pi_i(\boldsymbol{\theta}(t)) \mathbf{A}_i] \mathbf{x}(t) + \mathbf{B}_F F(t), \quad (6)$$

being \mathbf{A}_i all the vertex systems obtained by evaluating $\mathbf{A}(\boldsymbol{\theta})$ at θ_{v_i} , for $i = 1, \dots, N$.

V. VIC FORMULATION USING LMIs

Linear Matrix Inequalities (LMIs) have been increasingly used over the last decade to define many specifications in control design problems defined as convex optimisation ones [15]. In the particular case of polytopic LPV systems, LMIs can be formulated for every vertex system and related through a common Lyapunov candidate function in order to ensure properties for the complete range of operation of the system, i.e. all the values of $\boldsymbol{\theta}$. In other words, properties for the complete range of operation of a system can be assessed only by using a finite set of vertices models linked through a common solution. In this section, we go through all the LMI forms of the specifications used in the iterative controller assessment problem. As VICs will be implemented on a real platform with a control cycle T_c ($t = kT_c$), the problem is defined for the discrete-time form of system (3).

A. Stability

The first consideration when designing a controller to be safe is to guarantee stability, which ensures that the system is able to reach a steady-state under no external disturbances. In practice, this condition implies that improper behaviours, as e.g. increasing oscillations, ever happen due to the control strategy.

Proposition 1: Stability LMI for VIC polytopic LPV model. Considering the discrete-time polytopic LPV model of (6), the equilibrium $\mathbf{x} = 0$ is stable in the sense of Lyapunov for $k = [0, \infty) \in \mathbb{N}$ if there exist a solution matrix $\mathbf{P} > \mathbf{0} | \mathbf{P} = \mathbf{P}^T$ that fulfils the following LMI $\forall i = 1, \dots, N$:

$$\begin{bmatrix} -\mathbf{P} & \mathbf{P}\mathbf{A}_i^T \\ \mathbf{A}_i\mathbf{P} & -\mathbf{P} \end{bmatrix} \leq \mathbf{0}. \quad (7)$$

Proof: The proof is given in Appendix A.1. ■

B. Limits on position error and control effort

Restrictions on controller performance are key to successfully perform a task. In this paper, we consider two relevant constraints on determining performance for robots in anthropic domains: max. position deviation and control effort, i.e.

$$|\mathbf{u}_k| \leq u_{max}, \quad |e_k| \leq \Delta p_{max}; \quad (8a,b)$$

This implies that at each time-step k , for a limit position deviation of $\pm \Delta p_{max}$ w.r.t. p_k^r , control effort u_k will remain within $\pm u_{max}$.

Proposition 2: Maximum control effort and position error LMIs for VIC polytopic LPV model. Considering the problem in Prop. 1, constraints (8a) and (8b) are satisfied, respectively, if the following LMIs are fulfilled $\forall i = 1, \dots, N$:

$$\begin{bmatrix} u_{max}^2 \mathbf{I}_W & \mathbf{W}_i \mathbf{P} \\ \mathbf{P} \mathbf{W}_i^T & \mathbf{P} \end{bmatrix} \geq \mathbf{0}, \quad \begin{bmatrix} \mathbf{P} & \mathbf{P}\mathbf{A}_i^T \mathbf{S}^T \\ \mathbf{S} \mathbf{A}_i \mathbf{P} & \Delta p_{max}^2 \end{bmatrix} \geq \mathbf{0}; \quad (9a,b)$$

where \mathbf{S} is a selection matrix for $e(t)$; and such that

$$\begin{bmatrix} \mathbf{I}_0 & \mathbf{x}_0^T \\ \mathbf{x}_0 & \mathbf{P} \end{bmatrix} \geq \mathbf{0}; \quad (10)$$

being $\mathbf{x}_0 \equiv \mathbf{x}(0)$ and \mathbf{I}_0 an identity matrix of the appropriate dimensions.

Proof: The proof is given in Appendix A.2. ■

C. Maximum Overshooting

Related to performance is the transient response of the system, i.e. how it behaves until it reaches the steady state. In (stable) second-order systems like (1) exponentially decaying oscillation might appear, which is not desirable in a real platform. This phenomenon can be characterised by the Percentage Overshooting (PO), which corresponds to the maximum peak value of the system measured from the reference, as a function of damping ratio ξ . In this paper, we restrict the pole location¹ of the closed-loop system (3) to a discrete-complex plane that sets a max. overshooting.

Proposition 3: Maximum overshooting LMI for VIC polytopic LPV model. Considering the problem in Prop. 1, system (3) response will not surpass the maximum percentage overshoot \overline{PO} if the following LMI is fulfilled $\forall i = 1, \dots, N$:

$$\alpha \otimes \mathbf{P} + \beta \otimes (\mathbf{A}_i \mathbf{P}) + \beta^T \otimes (\mathbf{P} \mathbf{A}_i^T) \leq \mathbf{0} \quad (11)$$

being $\alpha = \text{diag}(\alpha_e, \alpha_v)$, $\beta = \text{diag}(\beta_e, \beta_v)$ defined according to [17] as follows:

$$\bar{\xi} = -\log(\overline{PO}/100)/\sqrt{\pi^2 + \log^2(\overline{PO}/100)}; \quad (12a)$$

$$\varphi = \cos^{-1}(\bar{\xi}), \quad a_0 = -e^{-\pi/\tan\varphi}; \quad (12b,c)$$

$$a_{se} = (1 + a_0)/2, a_e = (1 - a_0)/2; \quad (12d,e)$$

$$b_e = (b a_e)/\sqrt{a_e^2 - (a - a_{se})^2}; \quad (12f)$$

$$\gamma = \tan^{-1}(b/(1 - a)); \quad (12g)$$

where $\text{Re}(\mathbf{r}) = a$ and $\text{Im}(\mathbf{r}) = b$, being \mathbf{r} in the complex discrete plane belonging to the logarithmic spiral defined by φ .

Proof: The proof is given in Appendix A.3. ■

VI. VIC SOLUTION GENERATION

In this section, the integration of the LMI conditions as a convex optimisation problem together with user preference to generate a VIC solution is presented. First, we have to define the parameters of the VIC that define controller solution C_s . Considering the VIC structure and the LfD technique described in Section III, we have

$$C_s = \{K_{max}^s, K_{min}^s, D^s\}. \quad (13)$$

Therefore, taking into account that all the impedance parameters must remain positive, user only has to provide to the solution-search method a range $[\underline{K}, \overline{K}]$ for K_{max} and K_{min} and $[\underline{D}, \overline{D}]$ for D . Additionally, Eq. (2) implies the introduction of the constraint $K_{max} > K_{min}$ such that the compliance is adjusted by trajectory variance as intended.

A. Controller solution assessment with LMIs

Properties of each C_s are assessed through an optimisation problem including the LMI conditions presented in the previous section. In this case, we aim to obtain a stable VIC that presents an overshooting below or equal to \overline{PO} and a

¹Following [16], we define the poles of a LPV system as the set of all the poles obtained by freezing θ_{v_i} to all its possible values. Although this does not correspond with its standard definition for linear systems, this slight abuse of language is justified as it has been reported to have a connection with the dynamical behaviour of the LPV system.

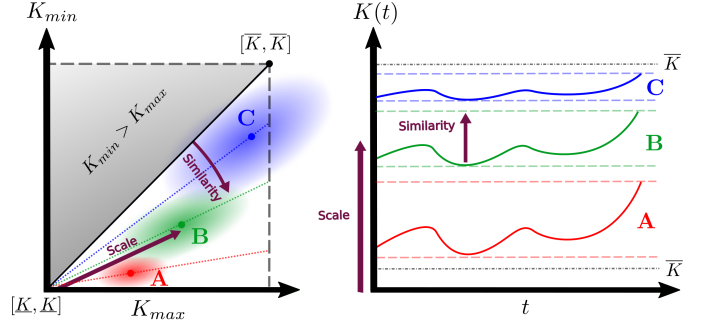


Fig. 2: Graphical representation of the User Preference mechanism for three different cases on the same compliance profile.

maximum position deviation Δp_{max} . Among all the solutions that fulfil these conditions (namely feasible), we will consider as optimal those that ensure a maximum control effort under $\overline{u_{max}}$, i.e. have the minimum guaranteed bound $u_{max} < \overline{u_{max}}$. This can be stated as the following optimisation problem for the discrete form of the polytopic LPV system (6):

$$\begin{aligned} &\text{For} && C_s \\ &\text{given} && \mathbf{x}_0, \overline{u_{max}}, \Delta p_{max}, \overline{PO}; \\ &\text{minimise} && u_{max}^2 \\ &\text{subject to} && (7), (9a,b), (10), (11). \end{aligned} \quad (14)$$

It should be noted that u_{max}^2 is the minimisation objective instead of u_{max} as it would make the problem non-convex.

B. User Preference mechanism

When performing a task with a robot, to obtain a satisfactory result is key to introduce human intuition. Regarding our method, the LfD technique only allows to specify the compliance profile through a set of demonstrations for the same task, but the user has no means to introduce the rigidity associated with each maximum and minimum level of compliance. In this paper, we have introduced an heuristic that biases the selection of the most optimal C_s towards desired compliance limits, namely User Preference. Particularly, we set this mechanism in the controller region defined by K_{max} and K_{min} through two intuitive parameters ranging in $[0, 1]$: Similarity and Scale. Similarity defines the "closeness" between K_{max} and K_{min} , and Scale where the profile remains within $[\underline{K}, \overline{K}]$. Mathematically, this is represented by a Gaussian that maps the tuple (K_{max}, K_{min}) to a value in $[0, 1]$, being the 0 value at its center. Similarity determines the angle between the diagonal $K_{max} = K_{min}$ and the direction of the major axis of the Gaussian function passing by $(\underline{K}, \underline{K})$. Its center is placed over this axis according to Scale considering the total length within the controller space limits. Thus, standard deviations of the Gaussian functions are assigned as half the distance between the center and the origin (major axis) and the intersection point with the controller space along its perpendicular (minor axis). In Fig. 2 a representation of this mechanism for three different User Preference sets on the same compliance profile.

Algorithm 1 VIC solution generation algorithm

Require:

H-GP data : $\mathbf{x}_0, \Delta p_{max}$
 Solution-search settings: $S_{search} = \{\underline{K}, \overline{K}, \underline{D}, \overline{D}\}$
 Solution-search constraints: $C_{search} = \{K_{max} > K_{min}\}$
 VIC definition : H
 LMI-problem settings : $S_{LMI} = \{\overline{u_{max}}, \overline{PO}\}$
 User Preference: Similarity, Scale

Ensure: $\hat{C}_s^* = C_s^*$ **repeat**

$C_s \leftarrow \text{Solution-Search}(S_{search}, C_{search})$
 $\mathbf{A}_i \leftarrow \text{Vertex Systems}(C_s, H)$ ▷ Eqs. 3,5
 $f_s^{LMI} \leftarrow \text{Opt. problem}(\mathbf{A}_i, \mathbf{x}_0, S_{LMI})$ ▷ In 14
 $f_s^{User} \leftarrow \text{User Preference}(C_s, \text{Similarity, Scale})$
 $f_s \leftarrow f_s^{LMI} + f_s^{User}$
 $\text{Solution-Search} \leftarrow \{C_s, f_s\}$
 $\{\hat{C}_s^*, \hat{f}_s^*\} \leftarrow \text{Solution-Search}$
until convergence

C. VIC solution generation

In this subsection, we describe the obtention of the optimal VIC controller solution C_s^* , summarised in Alg. 1. Before the beginning of the solution generation, all the necessary parameters must be provided. From the H-GP data, \mathbf{x}_0 is obtained considering that the robot is stalled at the beginning of the task, and Δp_{max} is defined as the minimum difference i.e. at the maximum stiffness level, between the confidence interval (95%) and the mean reference. User specifies the solution-search space S_{search} and the constraints within that space C_{search} (in this case $K_{max} > K_{min}$), together with desired inertia H , $\overline{u_{max}}$ and \overline{PO} and its preference in terms of Similarity and Scale. In the first step of the solution-generation algorithm, a solution candidate C_s is provided considering the ranges where parameters lie and the existing constraints between them. The set of vertex systems \mathbf{A}_i corresponding to C_s are computed using desired inertia H on the limit values for the varying parameter definition (Eq. 5) evaluated on the discrete form of \mathbf{A} (Eq. 3). Hence, they are used in the optimisation problem stated in (14) together with the settings for the LMI-constraints and the initial robot state \mathbf{x}_0 . For feasible solutions ², the optimality score f_s^{LMI} is obtained by scaling the minimum guaranteed control effort u_{max} in $[0, \overline{u_{max}}]$ to $[0, 1]$. Thus, the complete score f_s can be obtained as its sum with User Preference score f_s^{User} . Finally, C_s is associated with f_s in the solution-search method, that determines the most optimal solution \hat{C}_s^* with score \hat{f}_s^* from all the assessed solutions up to that iteration. This process is repeated until convergence criteria is met i.e. $\hat{C}_s^* \approx C_s^*$.

VII. VALIDATION

To validate the method presented in this paper, we perform a trajectory following task using a KINOVA GEN3 robotic

²Non-feasible ones (those that do not fulfil the all LMI-constraints simultaneously) are feed to the solution-search method to be taken into account when providing new solution candidates.

DoF Type	H [kg]	K [N/m]	D [N·s/m]
Translational	2	10000	$2 \cdot 0.8 \sqrt{K \cdot H}$
Rotational	1	1500	

TABLE I: Constant impedance controller gains for KINOVA GEN3 manipulator. Considering impedance is a 2nd-order dynamic behaviour, D is computed as a function of K and H with a damping ratio of 0.8.

manipulator for a planar (2-D) trajectory. A set of 10 trajectories representing a “wiping” movement have been obtained by guiding robot’s end-effector along a surface, from which the H-GP model (applied separately to each axis) provides the reference trajectory represented in Fig. 4a. Notice that every demonstration starts from a random position (within a range) in order to avoid null variability, which will imply infinite stiffness. To focus the attention on the behaviour of different controller solutions, the VIC is applied only for X-axis control, while constant impedance ones are used for remaining DoFs (Table I). From the H-GP covariance, represented in Fig. 4b by the 95% confidence intervals, the compliance profile determined by $\lambda(t)$ (Fig. 4c) is obtained, from which stiffness can be defined through K_{min} and K_{max} . The value of Δp_{max} is also obtained from the confidence interval being 3.19[cm] in this case. In order to exhibit the variant behaviour along the trajectory, a constant interaction force has been virtually introduced twice: in a high compliance (low stiffness) region between 2 and 4[s] and in a low compliance (high stiffness) region between 6.2 and 8.2[s]. In each of these regions, the compliant behaviours will be evaluated at certain point, namely Q1 and Q2. It should be noted that force magnitude is equal in both cases but in the first interaction is applied in the negative axis direction and then in the opposite one.

We have obtained solutions for four sets of User Preferences labelled as I-IV. For each one, four LMI-designs have been performed to analyse the effect of introduction each LMI-constraint into the controller generation. Thus, Design A has no constraints (only considers User Preference), Design B incorporates stability, Design C adds the limitation on position error and control effort, and finally Design D incorporates the max. overshooting constraint, i.e. the complete LMI problem as stated in (14). Thus, as for some controllers a safe execution can not be ensured, trajectory execution has been carried out in the physic-based simulator SIMSCAPE MULTIBODY within the MATLAB programming ecosystem, using the same constant control loop frequency of 1 [kHz] from the real platform. Regarding the LMI-design we have set $\overline{u_{max}} = 50$ [N] and $\overline{PO} = 5\%$. For all the controllers, desired inertia $H = 2$ [kg], K_{min} and K_{max} have been limited to $[0, 10000]$ [N/m] and D to $[0, 2500]$ [N·s/m] ³. For each User Preference - LMI-design combination, 10 solution controllers have been obtained to evaluate convergence under different initialisations, and among them the validation task has been performed by the one with the f_s^{User} closest to the mean. Table II provides the specific values for the chosen controller for execution for all the User Preference-LMI-Design combinations.

³As aforementioned, H must be determined regarding the characteristics of the robotic manipulator. All the upper bound values have been determined considering noise amplification.

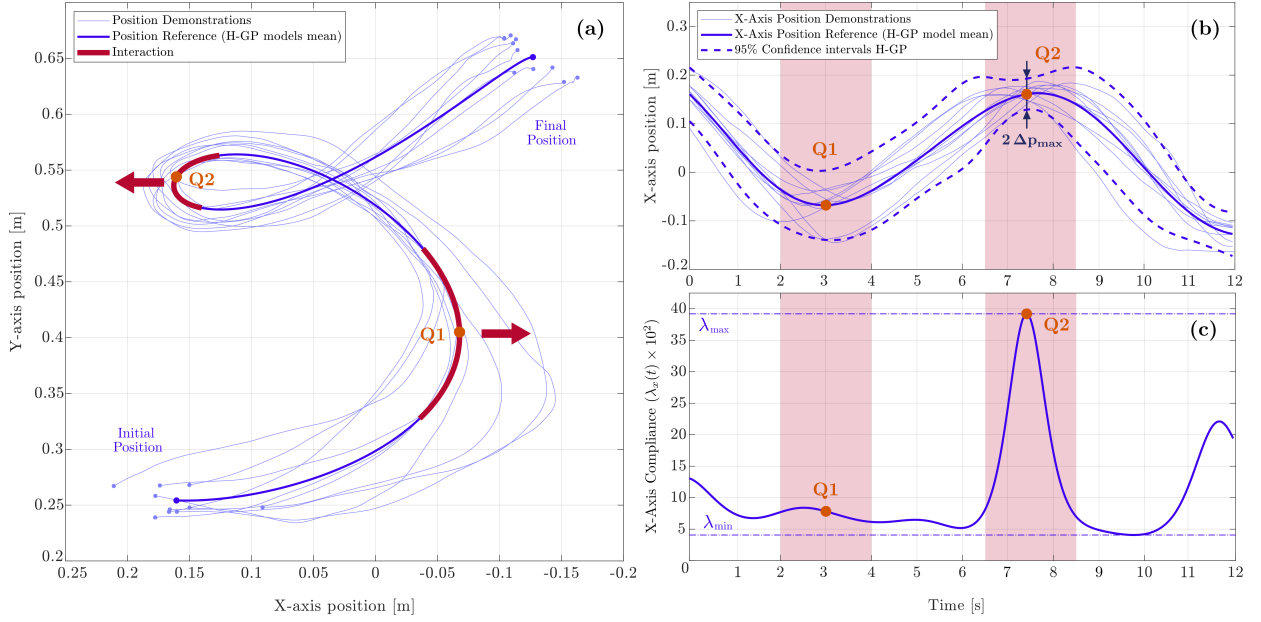


Fig. 3: Demonstrations of the validation trajectory and generated reference trajectory (a) together with the H-GP mean and confidence intervals for the X axis (b) and the corresponding compliance profile (c). Interaction regions where a constant force of 50[N] is applied in opposite directions are highlighted in the reference trajectory in (a) and represented as shadowed areas in (b) and (c), together with the points Q1 and Q2 where compliance has been evaluated.

Design	f_s^{User}	u_{\max} [N/kg]	K_{\max} [N/m]	K_{\min} [N/m]	D [N·s/m]
A	7.81×10^{-5}	-	4999	2086	2497
B	6.68×10^{-3}	-	4940	2067	2169
C	3.8×10^{-3}	4.61	5019	2181	71
D	7.24×10^{-2}	6.94	4803	1987	157

(a) User Preference I: Similarity = 0.5, Scale = 0.5

Design	f_s^{User}	u_{\max} [N/kg]	K_{\max} [N/m]	K_{\min} [N/m]	D [N·s/m]
A	9.02×10^{-4}	-	990	402	2455
B	1.43×10^{-4}	-	997	409	2416
C	3.13×10^{-2}	2.23	902	343	17
D	4.08×10^{-3}	2.87	988	431	65

(c) User Preference II: Similarity = 0.5, Scale = 0.1

Design	f_s^{User}	u_{\max} [N/kg]	K_{\max} [N/m]	K_{\min} [N/m]	D [N·s/m]
A	1.12×10^{-5}	-	9018	7671	2478
B	3.27×10^{-6}	-	8986	7687	139
C	2.35×10^{-2}	7.58	7814	7759	74
D	1.21×10^{-2}	7.83	8181	7847	177

(b) User Preference III: Similarity = 0.9, Scale = 0.9

Design	f_s^{User}	u_{\max} [N/kg]	K_{\max} [N/m]	K_{\min} [N/m]	D [N·s/m]
A	5.66×10^{-5}	-	8961	703	2016
B	1.92×10^{-3}	-	9261	721	1154
C	5.68×10^{-2}	5.55	7467	599	122
D	2.47×10^{-2}	7.75	8002	621	175

(d) User Preference IV: Similarity = 0.1, Scale = 0.9

TABLE II: Controller solutions for each User Preference - LMI Design combination, together with their corresponding value of User Preference score (f_s^{User}) and limit control effort (u_{\max}).

The dedicated webpage ⁴ contains implementation details together with a demo of the complete algorithm for the validation task. A video with the task execution for all the User Preference - LMI-designs is also available.

A. Results

Figure 4 shows the execution of the “wipping” task of all the obtained controllers. User Preference I sets a desired compliant behaviour centered in both Scale and Similarity ranges. Both controllers generated from Designs A and B present a highly damped behaviour along the task with respect to Designs C and D, due to the high values of D gain. In Fig. 4.I.a it can be seen how this produces a “slow” reaction during the first interaction: applying the external force drives the robot end-effector gradually away from the trajectory; when the force disappears these controllers take longer to reduce the tracking errors than controllers from Designs C and D. It has been

observed that for Designs A and B, D gain is randomly assigned by the solution generation method as they do not include LMI constraints able to fix its value. Regarding control effort (Fig. 4.I.b) this leads to an unbounded value that takes its highest value (considering the non-interaction sections of the trajectory) at the initial point. This does not happen with Designs C and D as they introduce a condition that provides an upper bound of the control effort (again, under no interaction) considering \mathbf{x}_0 . Between the controllers obtained from these two designs the most recognisable difference is the tracking behaviour (Fig. 4.I.a) when the external force is applied and fades out: while the controller from Design C presents a noticeable oscillatory response, the one from Design D presents a softened reaction. This difference becomes evident at the beginning of the second interaction. This is an effect of introducing the performance constraints while minimising the maximum control action, leading to low values of D that still fulfil the maximum deviation condition. By introducing the maximum overshooting condition in Design D, although

⁴ http://www.iri.upc.edu/groups/perception/#LMI_VIC_LfD

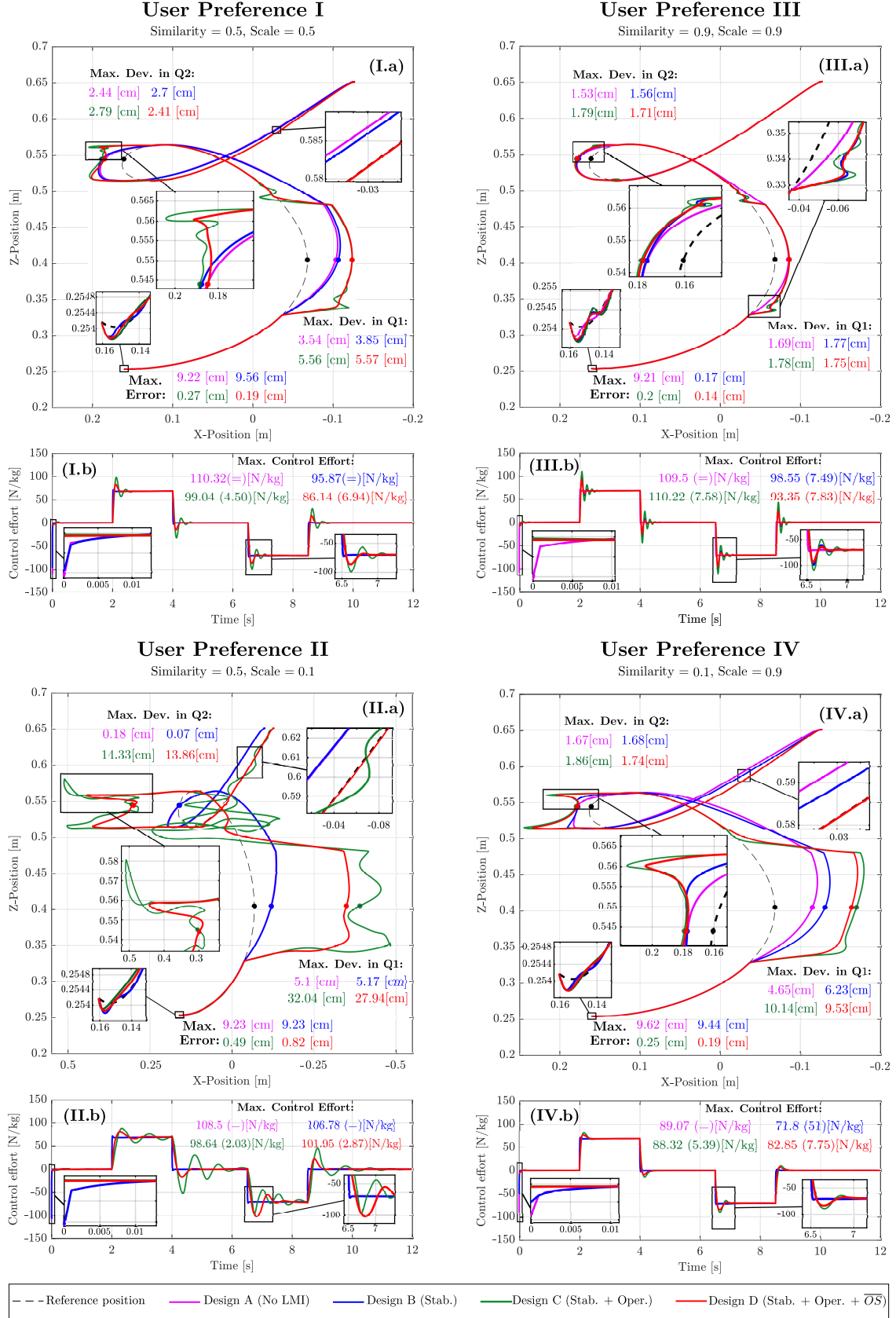


Fig. 4: Validation trajectory execution and control effort evolution using the VIC solution of each User Preference - LMI-design combination. For User Preference N, Figure N.a represents the end-effector position together with the maximum (abs.) trajectory error at the beginning of the task and deviations at Q1 and Q2, and Figure N.b depicts the evolution of the control effort and its maximum (abs.) values along the task and only without interaction (in parenthesis) are annotated.

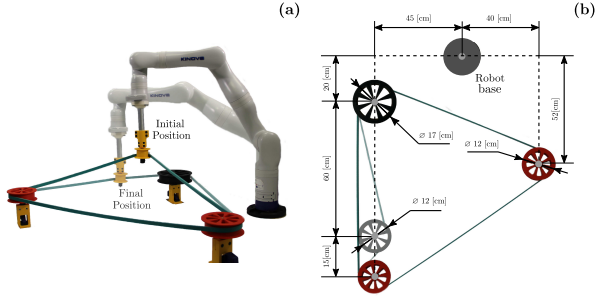


Fig. 5: Belt Drive unit setup for Case Study. Figure a depicts the initial and final (shadowed) positions of the KINOVA manipulator and belt configurations. Figure b includes the distribution of the pulleys w.r.t. the robot base, including the idler pulley (shadowed) for the first one-off modification scenario.

$\overline{u_{max}}$ is minimised, D is set to a higher value in order to reduce the oscillatory behaviour. This can also be observed for the control effort evolution in Fig.4.I.b. Note that in both Designs C and D, control effort evolution and max. error (both under no interaction) remain below LMI-design bounds in Table IIa.

Similar conclusions can be drawn for the remaining cases. From User Preference I to II Scale is reduced to 0.1 while similarity is maintained at 0.5. This generates solutions closer to the lower limits of the stiffness domain with Similarity again centered in the interval. Controllers from Designs A, B and D present similar characteristics than the ones obtained for User Preference I. With Design C, a lower D gain together with the low values of K_{min} and K_{max} due to scale causes an erratic behaviour on the second interaction, as it can be observed in Fig. 4.II.b. For User Preference III both similarity and scale increase to 0.9, which translates into high and similar values for K_{max} and K_{min} . Thus, the difference between deviations at Q1 and Q2 are the lowest (between 0.01 and 0.14 [cm]). In this case, all the controllers behave similarly for the tracking task (Fig. 4.III.a) but, again, the response under interaction from Design D controller is faster than from Design A controller but with less oscillations than Design C controller. Notice that in this case, controller obtained with Design B has almost the same behaviour as the one from Design D, due to their similar D . As with Design A, this gain is not fixed by any constraint and its value is randomly assigned. Finally, from User Preference III to IV only Similarity is changed to 0.1, which generates a variant controller solution that presents the greatest compliance differences along the task, being D the deviation in Q1 five times its value in Q2 for controller from Design C. In this case, controllers from Designs C and D have akin responses but oscillatory behaviour is still present with the controller from Design C, being most noticeable at the beginning of the first interaction. Finally note that both max. control effort and max. error bounds (Tables IIa - IIId) are also fulfilled by controller obtained with Designs C and D for all User Preferences II,III and IV.

VIII. CASE STUDY

Finally, we have evaluated the suitability of our method for a real scenario. Following the Assembly Challenge on the Industrial Robotics Category in World Robot Summit 2018 [18], we propose a belt drive unit where the task to be

Axis	f_s^{User}	u_{max} [N/kg]	K_{max} [N/m]	K_{min} [N/m]	D [N·s/m]
X	6.14×10^{-4}	9.38	4912	1181	128
Y	1.52×10^{-3}	4.69	4861	1169	160
Z	1.24×10^{-3}	4.86	5060	1241	158

(a) Nominal Scenario Controllers: Similarity = 0.3, Scale = 0.5

Axis	f_s^{User}	u_{max} [N/kg]	K_{max} [N/m]	K_{min} [N/m]	D [N·s/m]
X	2.22×10^{-4}	9.39	4934	4262	138
Y	1.08×10^{-3}	4.16	4989	4130	184
Z	3.78×10^{-2}	0.4	4646	4621	428

(b) Idler Pulley Scenario Controllers: Similarity = 0.9, Scale = 0.5

Axis	f_s^{User}	u_{max} [N/kg]	K_{max} [N/m]	K_{min} [N/m]	D [N·s/m]
X	2.75×10^{-3}	12.46	8674	2067	183
Y	2.75×10^{-2}	8.15	8081	2089	208
Z	2.01×10^{-2}	8.5	8148	1874	205

(c) Stiffer Belt Scenario Controllers: Similarity = 0.3, Scale = 0.9

TABLE III: Controller solutions for every axis in each case study scenario, together with their corresponding value of user preference term (f_s^{User}) and limit control effort (u_{max}).

performed is looping the belt over the last pulley (Figure 5). In this case, we want to apply the method presented in this paper in order to (i) make use of human knowledge on the task and (ii) reduce stress over the belt w.r.t. a constant rigid controller. Moreover, as in the Challenge, we present slight one-off modifications to evaluate the adaptability of the method to unseen new scenarios using the User Preference mechanism. The first scenario consists on the addition of an idler pulley (depicted in Figure 5b), the second one on using a stiffer belt than for the nominal setup.

We consider now the application of Variable Impedance Controllers for the translation control of the end-effector, namely in X, Y and Z-axis, while orientation impedance control remain with the same constant controllers as in the validation experiments (Table I). To obtain the H-GP model of the task, from 10 (random) initial position depicted in Fig. 5, a human operator hand-guides the robot end-effector (with a pulley adapter attached) to loop the belt over the final pulley. Figure 6a shows the representation of the reference trajectory and Figs. 6b-d show the compliance profile for X, Y and Z-axis, respectively. From them we can divide the task in a set of regions, depicted in all Figs. 6a-d from A to E.

In all of scenarios, we compare the performance of the controller in terms of the accumulated force exerted on the end-effector along all the directions, with respect to the execution using the constant impedance controllers from Table I. This is related with the elongation of the belt and, therefore, with its internal stress. The characteristics of all the controllers used in the Case Study are detailed in Table III. It should be mentioned that, in all scenarios, the same Scale and Similarity values have been used to design the controller in each axis, in order to present a better interpretation of the results and the User Preference mechanism. The values of Δp_{max} are 3.12 [cm] for X-axis, 2.03 [cm] for Y-axis and 0.55 [cm] for Z-axis. Remaining settings are maintained from validation experiments. All the results are reported in Fig. 7 and included in a video available in the dedicated webpage ⁴.

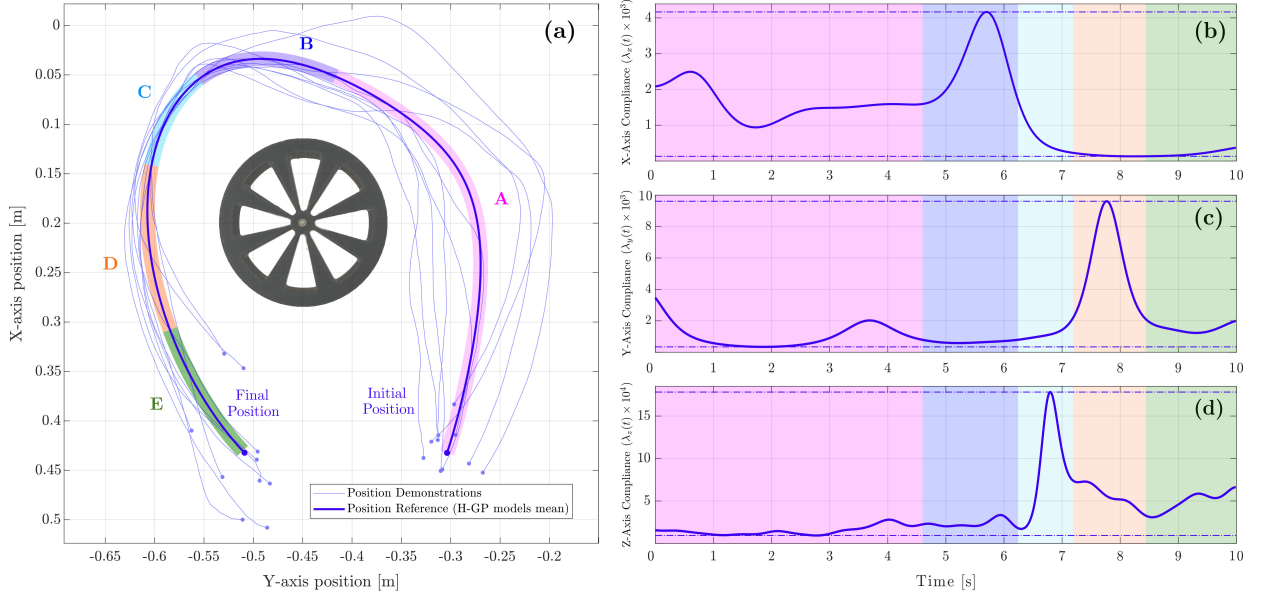


Fig. 6: Demonstrations of the looping task trajectory and generated reference trajectory (a) together with the corresponding compliance profiles in X (b), Y (c) and Z (d)-axes. The different task regions are highlighted in the reference trajectory in (a) and represented as shadowed areas in (b-d). Region A corresponds to the approach movement from the initial position to the pulley (low/medium stiffness in all three axis), Regions B to D to the stiffness maximum in X (beginning of the looping action), Z (ensure downwards movement is performed to engage belt) and Y-axes (avoid colliding the pulley), respectively. Region D to the last movement away from the pulley to the final position.

A. Nominal scenario

In this case we have chosen a Scale value of 0.5 to obtain a maximum stiffness value in the middle of the allowed range, and a Similarity value of 0.3 to emphasize the effect of the variant behaviour, i.e. increase the difference between K_{max} and K_{min} . As it can be seen in Fig. 7a-c, in all three axis, mean accumulated force is reduced w.r.t. the constant controller strategy between a 9% (X-axis) and a 14% (Z-axis). Looking at the normalized force difference it can be seen how stiffness modulation alters the exchanged force along the task. In Region A, the difference increases in all axis as the stiffness remains low, even though within the first two seconds the variant controller exerts higher forces in Y-axis (Fig. 7b) and Z-axis (Fig. 7c) that w.r.t. the variant approach (min. of -0.1). This might be an effect of the simultaneous control of multiple DoFs⁵. Then, in Region B, stiffness increase in X-axis does not present a noticeable effect in the force difference, but the same phenomena in Z-axis produces a reduction of the difference in Region C for all the axis, as the controller becomes stiffer for the end-effector to reach the desired height. At this point, it is worth remarking that the stiffness regulation in each axis propagates to all the other ones as they all affect the elongation of the belt. In Region D, stiffness peak in Y-axis maintains force difference in all axis, i.e. the controller holds rigid to maintain the position in Y at the cost of increasing exchanged force. Finally, force difference rises due to the stiffness reduction in all axes at Region E.

⁵Simultaneously introducing multiple control objectives for the same kinematic chain might incur in some deviation from the desired behaviour from one into the other. In this case, the constant orientation controllers might impose its behaviour over the variable ones when their stiffness is lower, which can be accentuated at the beginning due to the non-zero reference velocity. Multiple works acknowledge and tackle this problem, as e.g. [19]

B. Idler pulley scenario

The first one-off modification consists on introducing a complementary pulley that provides tension and guides the belt, namely idler. Using the same controller as in the nominal scenario does accomplish the task, but the belt slides over the upper face of the pulley when lowering the end-effector to the desired height, as it can be seen in Fig. 8a. This takes place between Regions C and D (7-7.5[s]), just before reaching the maximum stiffness in Y-axis. This means that the rigidity profile does not convey enough force to reach a position in Y-axis that avoids the impact. Therefore, in this case, we increase Similarity to 0.9 to bring the minimum stiffness closer to the maximum one. Applying the new controller, the task is performed without any issue and the reduction of the mean accumulated force in all three axis is reduced to values around 20%. Note that in this case, the normalized force difference profile has a more uniform behaviour along the task in comparison with the nominal scenario. This means that the behaviour is closer to a constant controller (in the same range of values), due to the closeness of K_{min} and K_{max} .

C. Stiffer belt scenario

For the second scenario, we change to a stiffer belt w.r.t. the one used on the nominal pulley configuration. In this case, using the controller designed for the nominal scenario does not lead to task fulfilment. As it can be seen in Fig. 8b, the belt is not looped over the last pulley as the controller does not provide enough effort to reach the required position before lowering to the desired height. This happens just after the stiffness peak in X-axis (6-6.5[s]), which means that even the maximum stiffness is not enough to counteract the forces from the stiffer belt. Thus, from the nominal User Preference, we increase Scale to 0.9 in order to increase both K_{max} and

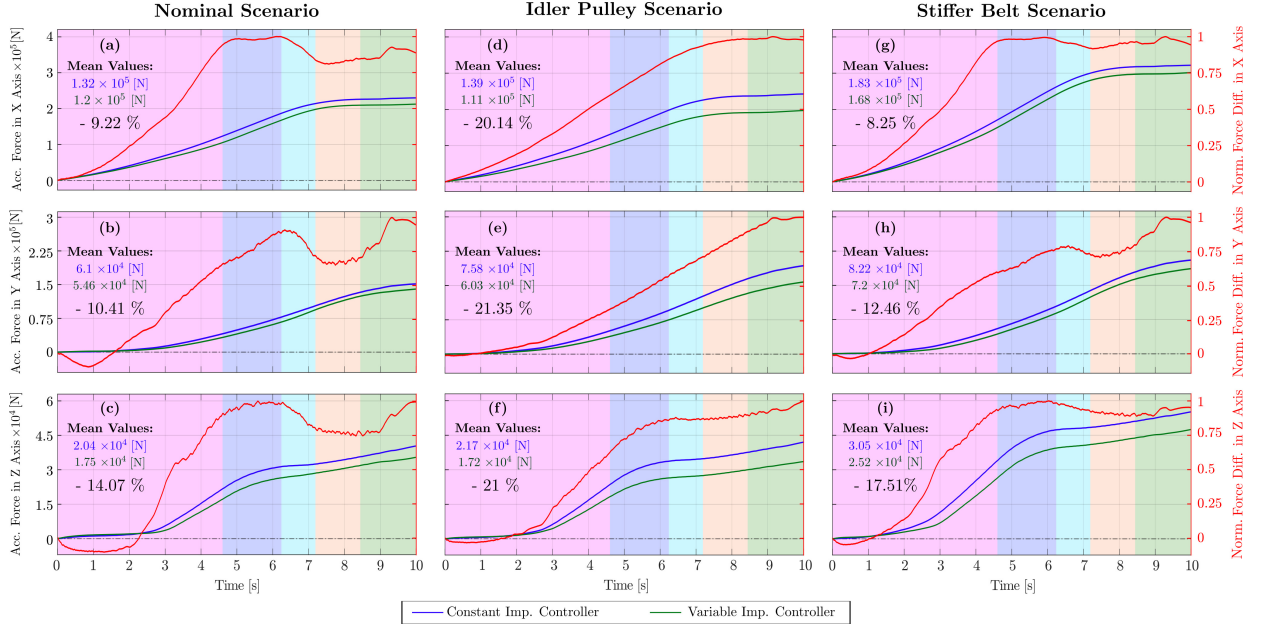


Fig. 7: Accumulated Force of the Constant and Variable Impedance Controller solutions together with the Normalized Difference (w.r.t. the maximum value) between them for X, Y and Z-axes on the three scenarios for the Belt Unit Case Study: Nominal (a-c), Idler Pulley (d-f) and Stiffer Belt (g-i). For each one, the mean accumulated force values and the reduction/increase the variable controller value represents over the constant one have been also included.

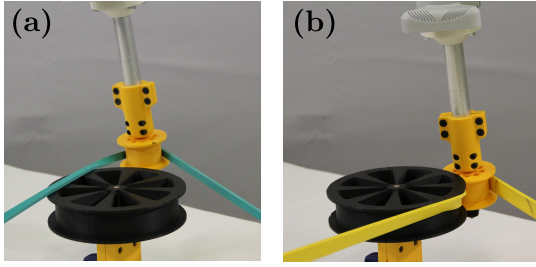


Fig. 8: Looping task execution errors from using the nominal controller solution (Table IIIa) on the Idler Pulley (a) and Stiffer Belt (b) scenarios.

K_{min} to greater values within the allowed range. This new set of controllers is able to complete the task while reducing the mean accumulated force to values between an 8% (X-axis) to a 17.5% (Z-axis). The normalized force difference profiles are akin to the ones obtained on the nominal scenario as both controllers have the same Similarity. As it can be seen in Tables IIIa and IIIc, this translates in a ratio of approx. 4 between K_{max} and K_{min} in both cases for all axes. Note also that, w.r.t. nominal scenario, the negative difference in the first two seconds (Figs. 7h,i) is reduced to a min. of -0.05. This might be due to the higher values at the lower stiffness region, which make the (variable) position controllers less prone to cross-effects from the simultaneous (constant) orientation controller.

IX. CONCLUSIONS

In this paper, we have presented a new off-line method to find the parameters of a VIC from a set of human-guided demonstrations, considering performance constraints and user preferences on compliant behaviour. First, user guides the robot multiple times along a trajectory to perform a task, from which compliance information can be extracted. In this case,

we took a well-known LfD technique that associates trajectory variability with stiffness level along time. Then, on one hand, performance constraints for the VIC are specified through a LMI-based design problem that requires a LPV formulation of the VIC. On the other hand, user preferences are introduced through Similarity and Scale terms to specify the behaviour on high and low compliance regions. Both elements are combined into a solution generation algorithm that iteratively finds the most optimal solution fulfilling the constraints and according to user preferences. Validation results in simulation show that the complete design generates controllers that are (i) stable, compliant and have a fast response without oscillations under interaction while (ii) fulfilling bounds on the control effort and maximum deviation and (iii) show the desired rigidity behaviour. We have also presented a Case Study where a real robot has to loop a belt over a pulley, where generated VIC solutions (i) reduce the accumulated total force to perform the task, even for one-off scenarios, where (ii) User Preference mechanism has been shown to have a key role in order to perform the task without any reconfiguration on the trajectory nor the control architecture.

APPENDIX

A. Proofs of LMI problem constraints

1) *Proof of Proposition 1:* The equilibrium point $\mathbf{x}_k = 0$ is stable in the sense of Lyapunov if there exists a discrete-time candidate function $V(\mathbf{x}_k)$ such that $\forall k \geq 0$: (i) $V(0) = 0$; (ii) $V(\mathbf{x}_k) \geq 0, \forall \mathbf{x}_k \neq 0$; and (iii) $V(\mathbf{x}_{k+1}) - V(\mathbf{x}_k) \leq 0, \forall \mathbf{x}_k \neq 0$. As stated in [20], applying the LMI approach for a quadratic candidate function $V(\mathbf{x}_k) = \mathbf{x}_k^T \mathbf{Q} \mathbf{x}_k$, above conditions are fulfilled iff there exist a solution matrix $\mathbf{Q} = \mathbf{Q}^T > 0$ such that:

$$\mathbf{A}_k \mathbf{Q} \mathbf{A}_k^T - \mathbf{Q} \leq 0 \quad (15)$$

For the discrete form of (6), defined by the system evaluated at Θ , Lyapunov stability implies that \mathbf{Q} is common to all the vertex state matrices, i.e. (15) is simultaneously fulfilled for all \mathbf{A}_i . Condition (7) is obtained by applying the Schur lemma [20] and the change of variable $\mathbf{P} = \mathbf{Q}^{-1}$, $\mathbf{P} = \mathbf{P}^T > 0$.

2) *Proof of Proposition 2:* Following [15], considering solution matrix $\mathbf{P} = \mathbf{P}^T > 0$ fulfilling (7) and introducing intermediate variable $\mathbf{L} = \sum_{i=1}^N [\pi_i(\theta(t)) \mathbf{W}_i] \mathbf{P}$, condition (8a) can be stated through the maximum norm of the control effort:

$$\begin{aligned} \|\mathbf{u}_k\|_2^2 &\leq \max_{k \geq 0} \|\mathbf{u}_k\|_2^2 = \max_{k \geq 0} \|\mathbf{L} \mathbf{P}^{-1} \mathbf{x}_k\|_2^2 \\ &\leq \max_{\mathbf{x}} \|\mathbf{L} \mathbf{P}^{-1} \mathbf{x}\|_2^2 \leq \overline{\sigma}(\mathbf{P}^{-1/2} \mathbf{L}^T \mathbf{L} \mathbf{P}^{-1/2}) \leq u_{\max}^2 \end{aligned}$$

Similarly, for operational constraint (8b):

$$\begin{aligned} \|e_k\|_2^2 &\leq \max_{k \geq 0} \|e_k\|_2^2 = \max_{k \geq 0} \|\mathbf{S} \mathbf{A} \mathbf{x}_{k-1}\|_2^2 \\ &\leq \max_{\mathbf{x}} \|\mathbf{S} \mathbf{A} \mathbf{x}\|_2^2 \leq \overline{\sigma}(\mathbf{P}^{1/2} (\mathbf{S} \mathbf{A})^T (\mathbf{S} \mathbf{A}) \mathbf{P}^{1/2}) \leq \Delta p_{\max}^2 \end{aligned}$$

Hence, applying Schur lemma [20] for the polytopic formulation leads to (9a) and to (9b) respectively. Note that \mathbf{S} is used to limit only the position error e_k considering the definition of state vector \mathbf{x}_k . Both (9b) and (8a) shape an invariant ellipsoid $\mathcal{E} = \{\mathbf{x}_k^T \mathbf{P}^{-1} \mathbf{x}_k < \mathbf{I}\}$ and (10) ensures that \mathbf{x}_0 belongs to \mathcal{E} by applying the Schur lemma on its definition.

3) *Proof of Proposition 3:* Condition (11) corresponds to the \mathbb{D} -stability definition [20], which is a generalisation of the Lyapunov stability to limit the eigenvalues of state matrix \mathbf{A}_k to a symmetric region \mathbb{D} in the complex plane defined through α and β . A max. percentage overshoot w.r.t. a reference value \overline{PO} in second order systems corresponds to a maximum damping ratio ξ as defined in (12a). This corresponds in the (discrete) complex plane to a logarithmic spiral, characterised by φ , which determines its intersection with the real axis a_0 as defined in Eqs. (12b,c). In [17], the non-convex region (namely cardioid) generated by these spirals is approximated by the intersection of two regions: an ellipsoid and a cone, defined in Eqs. (12a,b) and (12c,d) respectively. The ellipsoid is defined by its center a_{se} (Eq. (12d)) and its major and minor axes a_e (Eq. (12e)) and b_e (Eq. (12f)); and the cone with its vertex in (1,0) by half its inner angle γ (Eq. (12g)). The intersection point between regions $r = (a, b)$ must be specified such that it belongs to the logarithmic spiral. A value of $a = 0.95$ has been chosen for all the designs as it has been seen to provide a good approximation closer to (0,1).

REFERENCES

- [1] A. G. Billard, S. Calinon, and R. Dillmann, "Learning from humans," *Springer handbook of robotics*, pp. 1995–2014, 2016. (Cited on p. 1)
- [2] N. Hogan, "Impedance control: An approach to manipulation," in *Proceedings - IEEE ACC*, 1984, pp. 304–313. (Cited on p. 1)
- [3] F. J. Abu-Dakka and V. Kyrki, "Geometry-aware Dynamic Movement Primitives," *Proceedings - IEEE ICRA*, no. 2, pp. 4421–4426, 2020. (Cited on p. 1)
- [4] S. Calinon, I. Sardellitti, and D. G. Caldwell, "Learning-based control strategy for safe human-robot interaction exploiting task and robot redundancies," *Proceedings - IEEE/RSJ IROS*, pp. 249–254, 2010. (Cited on p. 2)
- [5] A. Behal, W. Dixon *et al.*, *Lyapunov-based control of robotic systems*. CRC Press, 2009. (Cited on p. 2)

- [6] E. Spyros-Papastavridis, P. R. Childs, and J. S. Dai, "Passivity Preservation for Variable Impedance Control of Compliant Robots," *IEEE/ASME Trans. on Mechatronics*, vol. 25, no. 5, pp. 2342–2353, 2020. (Cited on p. 2)
- [7] A. Billard, "On the mechanical, cognitive and sociable facets of human compliance and their robotic counterparts," *Rob. and Auton. Syst.*, vol. 88, pp. 157–164, 2017. (Cited on p. 2)
- [8] M. Bednarczyk, H. Omran, and B. Bayle, "Model predictive impedance control," *Proceedings - IEEE ICRA*, pp. 4702–4708, 1998. (Cited on p. 2)
- [9] M. Khansari, K. Kronander, and A. Billard, "Modeling robot discrete movements with state-varying stiffness and damping: A framework for integrated motion generation and impedance control," *Robotics: Science and Systems X*, jul 2014. (Cited on p. 2)
- [10] A. San-Miguel, G. Alenyà, and V. Puig, "Automated off-line generation of stable variable impedance controllers according to performance specifications," *IEEE RAL*, vol. 7, no. 3, pp. 5874–5881, 2022. (Cited on p. 2)
- [11] A. Dietrich, X. Wu *et al.*, "Practical consequences of inertia shaping for interaction and tracking in robot control," *Control Engineering Practice*, vol. 114, no. March, p. 104875, 2021. (Cited on p. 2)
- [12] K. Kersting, C. Plagemann *et al.*, "Most likely heteroscedastic gaussian process regression," *Proceedings - Int. Conf. Machine Learning*, pp. 393–400, 2007. (Cited on p. 2)
- [13] J. Mohammadpour and C. W. Scherer, *Control of Linear Parameter Varying Systems with Applications*. Springer US, 2012, vol. 148. (Cited on p. 3)
- [14] X.-D. Sun and I. Postlethwaite, "Affine LPV modelling and its use in gain-scheduled helicopter control," *Proceedings - UKACC Int. Conf. on Control*, pp. 1504–1509, 1998. (Cited on p. 3)
- [15] S. Boyd, L. El Ghaoui *et al.*, *Linear Matrix Inequalities in System and Control Theory*. SIAM, 1994. (Cited on p. 3, 11)
- [16] A. S. Ghersin and R. S. Pena, "LPV control of a 6-dof vehicle," *IEEE Transactions on Control Systems Technology*, vol. 10, no. 6, pp. 883–887, 2002. (Cited on p. 4)
- [17] D. Rosinová and M. Hypiusová, "LMI pole regions for a robust discrete-time pole placement controller design," *Algorithms*, vol. 12, no. 8, 2019. (Cited on p. 4, 11)
- [18] Y. Yokokohji, Y. Kawai *et al.*, "Assembly challenge: a robot competition of the industrial robotics category, world robot summit—summary of the pre-competition in 2018," *Advanced Robotics*, vol. 33, no. 17, pp. 876–899, 2019. (Cited on p. 8)
- [19] A. Dietrich, C. Ott, and A. Albu-Schaffer, "Multi-objective compliance control of redundant manipulators: Hierarchy, control, and stability," *Proceedings - IEEE/RSJ IROS*, pp. 3043–3050, nov 2013. (Cited on p. 9)
- [20] G.-R. Duan and H.-H. Yu, *LMIs in Control Systems*. CRC Press, jun 2013. (Cited on p. 10, 11)

Alberto San-Miguel received the B.Sc. degree in Industrial Engineering from University of Zaragoza, Spain, the M.Sc degree in Automatic Control and Robotics from Universitat Politècnica de Catalunya (UPC). He is currently pursuing his Ph. D. in Advanced Control Techniques for Interaction Control in Institut de Robòtica i Informàtica Industrial (IRI). His research interest include compliant control, controller design and human-robot interaction.

Guillem Alenyà received his Ph.D. degree (Doctor Europeus) from Universitat Politècnica de Catalunya (UPC) in 2007, supported by a EU-FP6 Marie-Curie scholarship. He is currently Researcher and Director at the Institut de Robòtica i Informàtica Industrial (IRI). His current research is devoted to facilitate the introduction of robots in human environments, principally in the fields of assistive robotics and garment manipulation. He is coordinator of various projects on developing enabling technologies for assistive robotics: ROB-IN, CLOE-GRAPH and principal investigator in the SeCuRoPS project and BURG. He has been coordinator of the SIMBIOTS and HuMoUR (co-IP F. Moreno) projects, and principal investigator of the SOCRATES project.

Vicenç Puig received his B.Sc./M.Sc. degree in telecommunications engineering in 1993 and his Ph.D. degree in Automatic Control, Robotics and Computer Vision in 1999, both from the Universitat Politècnica de Catalunya (UPC), Barcelona, Spain. He is a full professor at the Automatic Control Department of UPC and a researcher at the Institut de Robòtica i Informàtica Industrial (IRI). He is the director of the Automatic Control Department and the head of the Research Group on Advanced Control Systems (SAC) at UPC. He is currently the chair of the IFAC SafeProcess TC Committee 6.4. He was the general chair of the 3rd IEEE Conference on Control and Fault-Tolerant Systems (SysTol 2016) and the IPC chair of IFAC SafeProcess 2018. He has made important scientific contributions in the areas of fault diagnosis and fault tolerant control, using interval and linear-parameter-varying models exploiting set-based approaches.